Geochemical Perspectives Letters

Core-mantle chemical interaction *via* convection within thermochemical piles

J. Korenaga, S. Marchi

Supplementary Information

The Supplementary Information includes:

- Modeling Thermochemical Piles in Whole Mantle Convection
- Quantifying the Efficiency of Transporting Core Signatures
- Figures S-1 and S-2
- Supplementary Information References

Modeling Thermochemical Piles in Whole Mantle Convection

Governing equations and boundary conditions

The convection modeling reprocessed here is based on the nondimensionalized governing equations for thermal convection of an incompressible fluid, consisting of the conservation of mass, momentum, and energy (see Korenaga and Marchi, 2023, for these equations). The spatial coordinates are normalized by the mantle depth D (=2900 km), and time is normalized by the diffusion time scale, D^2/κ, where κ is thermal diffusivity (=10^{-6} m^2 s^{-1}). Temperature is normalized by a potential temperature difference between the surface and the core-mantle boundary, ΔT (=2000 K). The Rayleigh number Ra is defined here as:

$$Ra = \frac{\alpha \rho_0 g \Delta T D^3}{\kappa \eta_0},$$

where α is thermal expansivity (= 10^{-5} K^{-1}), ρ_0 is reference density (= 5000 kg m^{-3}), g is gravitational acceleration, and η_0 is the reference viscosity. Nondimensional heat generation is defined as:

$$H^* = \frac{\rho_0 H D^2}{k \Delta T},$$

where H is heat production rate per unit mass, and k is thermal conductivity. We tested a few values of H^* to achieve Earth-like internal heating rate (~0.6–0.7), which includes the effect of secular cooling (Korenaga, 2017). Viscosity is both temperature- and depth-dependent. The temperature dependence is prescribed by:

$$\eta_T^* = \exp[\theta(1 - T^*)],$$

where θ is called the Frank-Kamenetskii parameter, and the reference viscosity for the bottom three quarters of the mantle is raised by a factor of 30 (Hager, 1984).

The above governing equations are solved with the two-dimensional finite element code of Korenaga and Jordan (2003). The top and bottom boundaries are free slip. The top and bottom (nondimensional) temperatures are set to 0 and 1, respectively. A reflecting (*i.e.* free slip and insulating) boundary condition is applied to the side boundaries. The aspect ratio of a model is four to reduce wall effects, and the model is discretized by 400×100 uniform quadrilateral elements. Internal temperature is set to 0.7 at $t^* = 0$ with random perturbations of small amplitude (10^{-3}), and the system is integrated until $t^* = 0.0169$, which corresponds to 4.5 billion years.

Chemical tracers

The chemical composition is tracked by 10^8 tracers, which are initially randomly distributed and are advected with a fourth-order Runge-Kutta scheme (Christensen and Yuen, 1984). A certain fraction of these tracers are associated with a density anomaly of 4000 kg m^{-3} to represent metallic components. For a total metal mass of 10^{22} kg, for example, 0.25% of the tracers (2.5×10^5 tracers) are marked as dense tracers. Based on the results of three-phase flow modeling of Korenaga and Marchi (2023), such dense tracers are distributed at mid-mantle depths, corresponding to the location of a hypothetical partially molten zone. With a total metal mass of 10^{22} kg, a laterally homogeneous, 750-km thick partially molten zone would have an average metal concentration of ~0.97 wt%, and because metal concentration is expected to vary linearly within the zone, dense tracers are distributed so that the concentration is ~1.93 wt% at the top of the zone and linearly decreases to zero at its bottom. This would correspond to the case of a 3% Earth mass impactor with an impact angle of 45° and v/v_e=2.2 (Korenaga and Marchi, 2023; see their Table S3). We tested seven different initial tracer distributions. Four of them are with laterally homogeneous partially molten zones, all with the total metal mass of 10^{22} kg, the complete mixing of which would reproduce the present-day mantle abundance of HSEs. The thickness of the zone is 250 km (Case 1), 500 km (Case 2), 750 km (Case 3), and 1000 km (Case 4). The rest of the cases all have a 1000-km thick partially molten zone with a locally deep, 500-km thick partially molten zone for the mid-50% of the lateral extent. The total amount of metal in the deep zone is the same as that in the shallow zone in Case 5, and it is greater by 25% in Case 6 and 50% in Case 7. Thus, the total metal mass is 1.13×10^{22} kg in Case 6 and 1.25×10^{22} kg in Case 7.

Notes on modeling strategy

One of the important questions about the dynamics of thermochemical piles is how dense piles are entrained by the upwelling of the ambient mantle. The competition between thermal and chemical buoyancies near the core-mantle boundary region determines the efficiency of such convective entrainment, and this is the rationale behind the values adopted for thermal expansivity (10^{-5} K^{-1}) and reference density (5000 kg m^{-3}), both of which are appropriate for the lowermost mantle. We tested two Rayleigh numbers, 10^7 and 3×10^7, and with these material properties, they correspond to the reference viscosity of 2.4×10^{21} Pa s and 8×10^{20} Pa s, respectively.

For each of the two Rayleigh numbers, we have tested all of the seven initial tracer distributions, two internal heat production (20 and 25 for Ra=10^7, and 25 and 30 for Ra=3×10^7), and three Frank-Kamenetskii parameters (4.61, 5.70, and 6.91, which corresponds to the total viscosity contrast due to temperature of 10^2, 3×10^2, and 10^3, respectively), amounting to a total of 84 model runs. In general, greater temperature dependence of viscosity brings the system closer to stagnant lid convection, thereby decreasing the mixing efficiency as well as the surface heat flux (Korenaga and Marchi, 2023; see their Figure S3). For example, with the Frank-Kamenetskii parameter θ of 6.91, only ~20 to ~50% of the original thermochemical piles is eventually entrained, whereas with θ of 4.61, the entrainment efficiency is generally doubled.

We use the same temperature dependence of viscosity for both the upper mantle and lower mantle, and this may appear as a gross simplification. However, using a more complicated setting of mantle rheology does not necessarily yield more useful modeling results, because our primary goal is to understand the long-term dynamics of thermochemical piles. To simulate long-term convective interactions between the ambient mantle and thermochemical piles, it is important to maintain subduction and thus plate tectonics. If the mode of mantle convection is instead stagnant lid convection, convective currents in the mantle are characterized by small-scale thermal anomalies, which would reduce the efficiency of convective entrainment. We can avoid stagnant lid convection, either by using weak enough temperature-dependent viscosity or by using the combination of strongly temperature-dependent viscosity with some weakening mechanisms (*e.g.*, Bercovici *et al*., 2015), and we use the former for simplicity. The latter would be important if we are interested in simulating plate tectonics in more detail (*e.g.*, reproducing the high 'plateness'). The detailed rheology of the lower mantle is still largely unknown. From the studies of instantaneous Stokes flow and postglacial rebound, it is generally agreed that the lower mantle has a higher average viscosity (by a factor of 10 to 100) than the upper mantle (*e.g.*, Hager, 1984; Forte *et al*., 2015), but further details are subject to debate. Even the sign of the temperature dependence of viscosity is not settled yet, and the Frank-Kamenetskii parameter θ can be negative in the lower mantle (Solomatov, 1996, 2001; Korenaga, 2005; Frazer and Korenaga, 2022). We have varied the parameter θ from 4.61 to 6.91, to examine the sensitivity of our modeling results to the temperature dependence of viscosity, without implying which one would be most realistic. The cases with θ of 4.61 are generally most effective in entraining thermochemical piles, thus raising the mantle abundance of highly siderophile elements to a satisfactory level. This by itself does not mean that the actual temperature dependence of lower mantle viscosity is well represented by this value

of the Frank-Kamenetskii parameter. Nevertheless, this value of θ does correspond to a reasonable viscosity structure of the mantle. With the Rayleigh number of 3×10^7 or the reference viscosity of 8×10^{20} Pa s, the viscosity at the CMB (*i.e.* T^* = 1) is 2.4×10^{22} Pa s because the lower mantle is set to be 30 times more viscous than the upper mantle. With the temperature contrast of 2000 K across the entire mantle and the present-day potential temperature of 1350 K (Herzberg *et al*., 2007), the temperature contrast across the core-mantle boundary region is 750 K, so with θ of 4.61, the viscosity of ambient lower mantle is $\sim1.3\times10^{23}$ Pa s, which is within the estimated range for the mid-lower mantle viscosity based on instantaneous Stokes flow and postglacial rebound ($\sim2\times10^{22}$ Pa s to $\sim5\times10^{23}$ Pa s) (Forte *et al*., 2015; see their Figure 9) (see also our Figure S-2).

In a similar spirit, other aspects of our convection model are also kept simple; we do not change the temperature contrast across the mantle nor the amount of internal heating. In reality, the temperature contrast should decrease with time because of core cooling. It is not obvious how internal heating would change with time because, as mentioned earlier, internal heating in our model includes both radiogenic heating and secular cooling, so it does not have to monotonically decay with time. Varying the temperature contrast as well as internal heating with time can be done by modeling fully transient mantle convection coupled with the thermal history of the core, but this would inevitably increase the number of poorly constrained model parameters. For example, a hotter mantle in the past does not necessarily mean a less viscous mantle even with a positively temperature-dependent viscosity. Mantle viscosity is also sensitive to the water content (*e.g.*, Karato and Wu, 1993), and the water content of the mantle does not have to be constant with time. In fact, the deep water cycle indicates that the mantle is likely to have been drier in the past (Korenaga *et al*., 2017), which can offset the effect of higher temperature on mantle viscosity (Korenaga, 2011).

Quantifying the Efficiency of Transporting Core Signatures

For 2-D steady-state convection in a closed domain, the streamlines form nested closed loops. The outermost streamline coincides with the domain boundaries, and the parcels that originate at the bottom boundary traverse along all other boundaries. That is, when the base of the bottom boundary layer is brought to the surface by upwelling, it becomes the top of the top boundary layer. A similar situation may be expected for inter-pile convection, and core-affected mantle parcels may be efficiently exposed along the top and side boundaries of the piles. To quantify this, we adopt the following procedure. For each trajectory of entrained dense tracers, we measure its minimum distance to the CMB, and the cumulative distribution of the minimum distance is fitted with the cumulative exponential distribution, $1-\exp(-\lambda z)$, where z is the distance in km and λ is the fitting parameter. Fitting to a cumulative distribution is to make this statistical inference less dependent on model resolution (*e.g.*, the number of tracers involved). For this fitting, we only consider the part of the cumulative distribution that is within the thickness of the bottom boundary layer, which is estimated from the transit time scale as $h \sim 2p\kappa\tau_T/2$. This exponential distribution is compared with the uniform distribution from z =

0 to $z = h$. The slope of the cumulative exponential distribution at $z = 0$ is λ itself, and that of the cumulative uniform distribution is $1/h$. We define the amplification factor as the ratio of these two slopes, *i.e.* λh.

Supplementary Figures

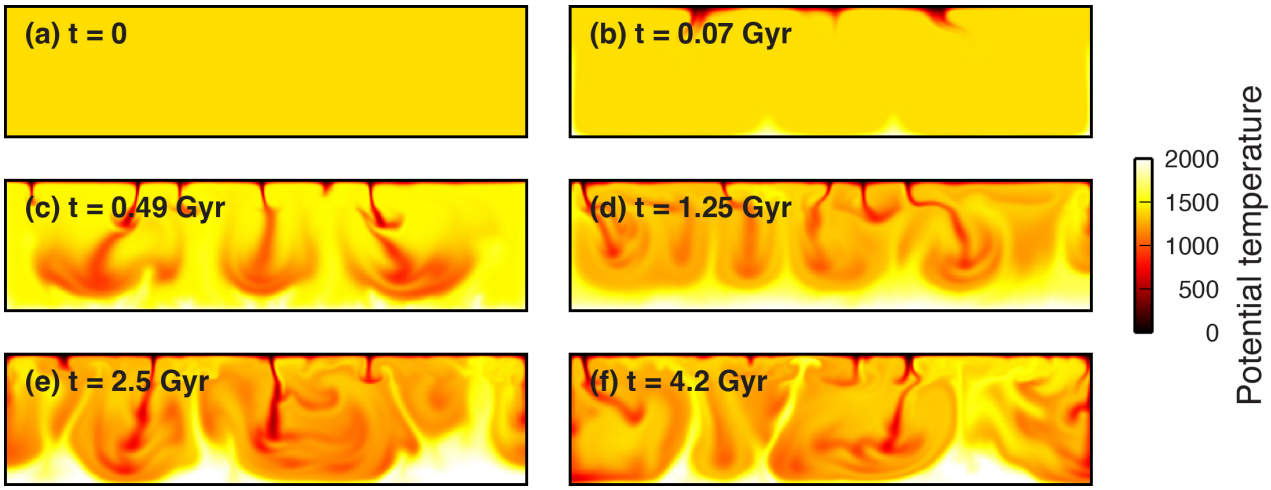

Figure S-1 Snapshots of the temperature field corresponding to those of the composition field shown in Figure 1.

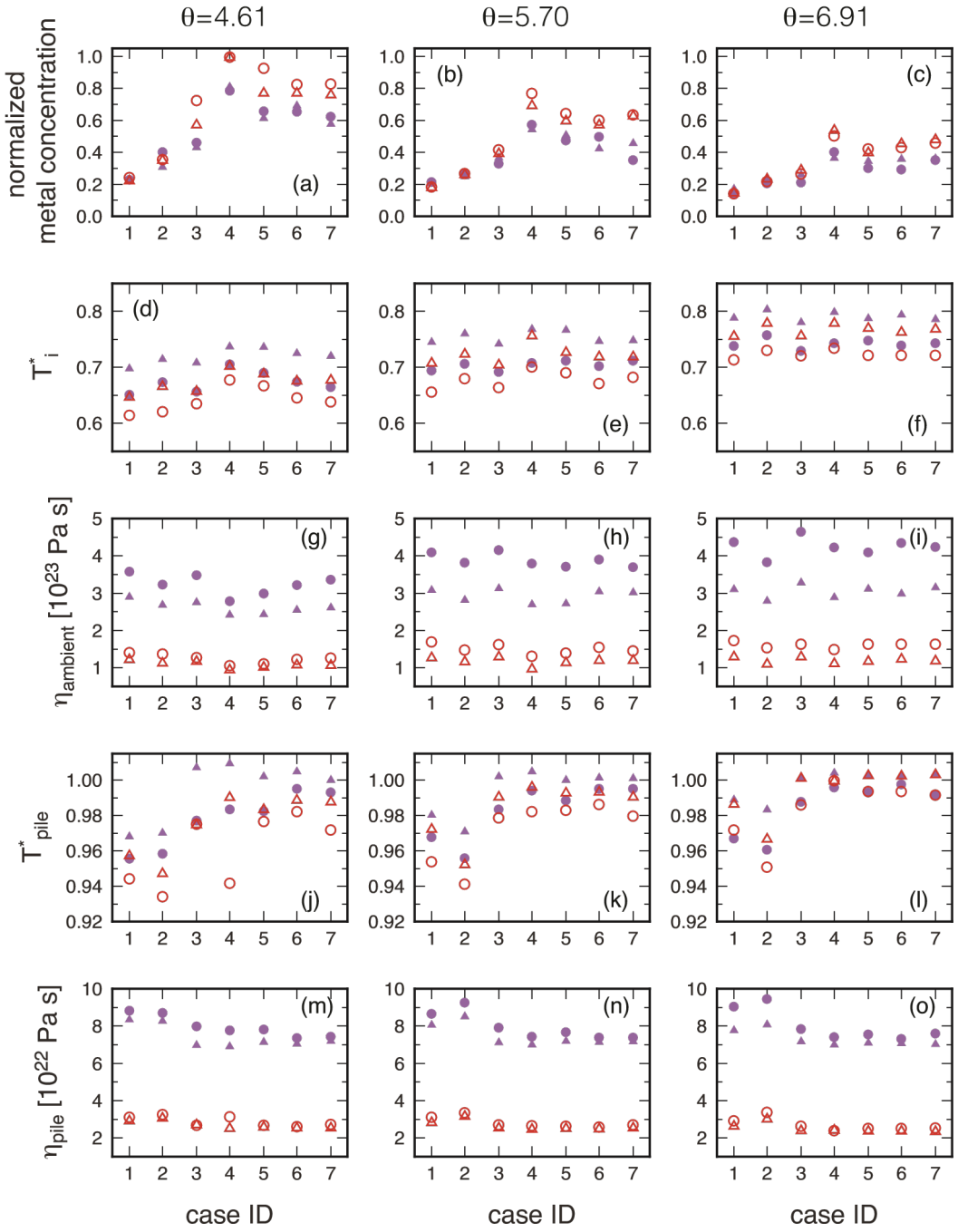

Figure S-2 Diagnostics of convection model runs. The first through the fifth columns show, respectively, normalized metal concentration in the upper mantle (unity corresponding to the observed level) measured at t =4.5 Gyr (present), nondimensional internal temperature, the viscosity of ambient lower mantle, nondimensional pile temperature, and the viscosity of pile. The latter four quantities are time-average from 1 Gyr to 4.5 Gyr. Left, middle, and right columns correspond to different values of the Frank-Kamenetskii parameter as shown. Solid and open symbols are for Ra = 10^7 and 3×10^7, respectively, and circles and triangles denote low and high values for internal heat generation, respectively. See Figure S3 of Korenaga and Marchi (2023) for internal heating ratio and surface heat flux.

Supplementary Information References

Bercovici, D., Tackley, P.J., Ricard, Y. (2015) 7.07 - The Generation of Plate Tectonics from Mantle Dynamics. In: Schubert, G. (Ed.) *Treatise on Geophysics*. Second Edition, Elsevier, Amsterdam, 7, 271–318. https://doi.org/10.1016/B978-0-444-53802-4.00135-4

Christensen, U.R., Yuen, D.A. (1984) The interaction of a subducting lithospheric slab with a chemical or phase boundary. *Journal of Geophysical Research: Solid Earth* 89, 4389–4402. https://doi.org/10.1029/JB089iB06p04389

Forte, A.M., Simmons, N.A., Grand, S.P. (2015) 1.27 - Constraints on Seismic Models from Other Disciplines - Constraints on 3-D Seismic Models from Global Geodynamic Observables: Implications for the Global Mantle Convective Flow. In: Schubert, G. (Ed.) *Treatise on Geophysics*. Second Edition, Elsevier, Amsterdam, 1, 853–907. https://doi.org/10.1016/B978-0-444-53802-4.00028-2

Frazer, W.D., Korenaga, J. (2022) Dynamic topography and the nature of deep thick plumes. *Earth and Planetary Science Letters* 578, 117286. https://doi.org/10.1016/j.epsl.2021.117286

Hager, B.H. (1984) Subducted slabs and the geoid: Constraints on mantle rheology and flow. *Journal of Geophysical Research: Solid Earth* 89, 6003–6015. https://doi.org/10.1029/JB089iB07p06003

Herzberg, C., Asimow, P.D., Arndt, N., Niu, Y., Lesher, C.M., Fitton, J.G., Cheadle, M.J., Saunders, A.D. (2007) Temperatures in ambient mantle and plumes: Constraints from basalts, picrites, and komatiites. *Geochemistry, Geophysics, Geosystems* 8, Q02006. https://doi.org/10.1029/2006GC001390

Karato, S.-I., Wu, P. (1993) Rheology of the Upper Mantle: A Synthesis. *Science* 260, 771–778. https://doi.org/10.1126/science.260.5109.771

Korenaga, J. (2005) Firm mantle plumes and the nature of the core–mantle boundary region. *Earth and Planetary Science Letters* 232, 29–37. https://doi.org/10.1016/j.epsl.2005.01.016

Korenaga, J. (2011) Thermal evolution with a hydrating mantle and the initiation of plate tectonics in the early Earth. *Journal of Geophysical Research: Solid Earth* 116, B12403. https://doi.org/10.1029/2011JB008410

Korenaga, J. (2017) Pitfalls in modeling mantle convection with internal heating. *Journal of Geophysical Research: Solid Earth* 122, 4064–4085, doi:10.1002/2016JB013850. https://doi.org/10.1002/2016JB013850

Korenaga, J., Jordan, T.H. (2003) Physics of multiscale convection in Earth's mantle: Onset of sublithospheric convection. *Journal of Geophysical Research: Solid Earth* 108, 2333. https://doi.org/10.1029/2002JB001760

Korenaga, J., Marchi, S. (2023) Vestiges of impact-driven three-phase mixing in the chemistry and structure of Earth's mantle. *Proceedings of National Academy of Sciences* 120, e2309181120. https://doi.org/10.1073/pnas.2309181120

Korenaga, J., Planavsky, N.J., Evans, D.A.D. (2017) Global water cycle and the coevolution of Earth's interior and surface environment. *Philosophical Transactions of the Royal Society A* 375, 20150393. https://doi.org/10.1098/rsta.2015.0393

Solomatov, V.S. (1996) Can hotter mantle have a larger viscosity? *Geophysical Research Letters* 23, 937–940. https://doi.org/10.1029/96GL00724

Solomatov, V.S. (2001) Grain size-dependent viscosity convection and the thermal evolution of the Earth. *Earth and Planetary Science Letters* 191, 203–212. https://doi.org/10.1016/S0012-821X(01)00426-5